Alzheimer's & Dementia®
THE JOURNAL OF THE ALZHEIMER'S ASSOCIATION

FEATURED ARTICLE

The P522R protective variant of PLCG2 promotes the expression of antigen presentation genes by human microglia in an Alzheimer's disease mouse model

Christel Claes[1,2] 🔵 | Whitney E. England[3] | Emma P. Danhash[1,2] | Sepideh Kiani Shabestari[2,4] | Amit Jairaman[5] | Jean Paul Chadarevian[1,2,4] | Jonathan Hasselmann[1,2,4] | Andy P. Tsai[6] | Morgan A. Coburn[4] | Jessica Sanchez[4] | Tau En Lim[1] | Jorge L. S. Hidalgo[1] | Christina Tu[2] | Michael D. Cahalan[5] | Bruce T. Lamb[6,7] | Gary E. Landreth[6,8] | Robert C. Spitale[3] | Mathew Blurton-Jones[1,2,4] | Hayk Davtyan[1,2]

[1] Institute for Memory Impairments and Neurological Disorders, University of California Irvine, Irvine, California, USA

[2] Sue and Bill Gross Stem Cell Research Center, University of California Irvine, Irvine, California, USA

[3] Department of Pharmaceutical Sciences University of California, Irvine, California, USA

[4] Department of Neurobiology and Behavior, University of California Irvine, Irvine, California, USA

[5] Department of Physiology and Biophysics, University of California Irvine, Irvine, California, USA

[6] Stark Neurosciences Research Institute, IUSM, Indianapolis, Indiana, USA

[7] Department of Medical and Molecular Genetics, IUSM, Indianapolis, Indiana, USA

[8] Department of Anatomy and Cell Biology, IUSM, Indianapolis, Indiana, USA

Correspondence
Christel Claes, University of California Irvine, 3200 Gross Hall, 845 Health Sciences Rd, Irvine, CA 92697, USA.
E-mail: cclaes@uci.edu

Mathew Blurton-Jones and Hayk Davtyan contributed equally to this study.

Abstract

The P522R variant of PLCG2, expressed by microglia, is associated with reduced risk of Alzheimer's disease (AD). Yet, the impact of this protective mutation on microglial responses to AD pathology remains unknown. Chimeric AD and wild-type mice were generated by transplanting PLCG2-P522R or isogenic wild-type human induced pluripotent stem cell microglia. At 7 months of age, single-cell and bulk RNA sequencing, and histological analyses were performed. The PLCG2-P522R variant induced a significant increase in microglial human leukocyte antigen (HLA) expression and the induction of antigen presentation, chemokine signaling, and T cell proliferation pathways. Examination of immune-intact AD mice further demonstrated that the PLCG2-P522R variant promotes the recruitment of CD8+ T cells to the brain. These data provide the first evidence that the PLCG2-P522R variant increases the capacity of microglia to recruit T cells and present antigens, promoting a microglial transcriptional state that has recently been shown to be reduced in AD patient brains.

KEYWORDS
CCL8, chimeric Alzheimer's mouse model, human leukocyte antigen, human stem cell-derived microglia, MHCII, PLCG2, T cells

1 | NARRATIVE

Microglia are strongly implicated in the development and progression of Alzheimer's disease (AD).[1–5] Recently, the PLCG2 missense variant Pro522Arg (P522R), predominantly expressed by microglia within the brain, was shown to be associated with a reduced risk of developing late-onset AD.[6] PLCG2 has also been shown to be a downstream component of TREM2 signaling, an important microglial AD risk gene.[7,8] However, the impact of PLCG2-P522R on human microglial function in vivo and the mechanisms by which this variant reduces AD risk remains largely unknown. We therefore sought to examine the effect of the P522R variant on human microglia in a chimeric AD mouse model with the goal of addressing a major unanswered question in the field: How does the P522R variant affect the transcriptome of human microglia in vivo as they respond to amyloid pathology, and how might these changes lead to reduced AD risk?

PLCG2 encodes an enzyme belonging to the phospholipase C-gamma family, with functions including the cleavage of membrane phospholipid PIP2 (1-phosphatidyl-1D-myo-inositol 4,5-bisphosphate) into secondary messengers IP3 (myo-inositol 1,4,5-trisphosphate) and DAG (diacyl-glycerol). IP3 and DAG in turn propagate a wide range of signals, including release of calcium from endoplasmic reticulum (ER) stores, which in turn influences microglial gene expression, phagocytosis, cell survival, and chemotaxis.[9] In vitro studies have demonstrated that the P522R variant induces a slight increase in cytosolic calcium, both basally and upon stimulation, indicating mild hypermorphic activity.[10–12] In addition, depletion of intracellular calcium stores activates a calcium flux across the plasma membrane, referred to as store-operated calcium entry (SOCE), which is also moderately increased by the P522R variant in HEK293T cells.[10] Collectively, these changes are associated with improved survival, enhanced phagocytic/endocytic activity, and increased acute inflammatory response.[11,12] Despite this recent progress, studies of the P522R variant in vivo have thus far remained limited to the examination of wild-type (non-AD) P522R knock-in (KI) mice, which reported a trend toward increased expression of Cst7, Tyrobp, Clec7a, and Ccl3 by quantitative polymerase chain reaction of total brain mRNA.[11,12]

To further advance our understanding of the impact of the PLCG2 P522R variant on human microglia in AD, we generated a pair of isogenic PLCG2 wild-type (WT) and homozygous PLCG2-P522R human induced pluripotent stem cell (iPSC) lines via CRISPR/Cas9 and differentiated them into hematopoietic progenitors (HPCs) and microglia (iMGs).[13] Upon confirmation that introduction of the P522R mutation produces a hypermorphic effect on calcium signaling, significantly increasing resting calcium levels and store-operated calcium entry, we transplanted HPCs into our recently described WT and AD chimeric mouse models[14] and xenografted human iPSC-derived microglia (xMGs) matured and remained within recipient brains for 7 months, until they were isolated for single-cell (scRNA-seq) and bulk RNA sequencing. Our results indicate that human iPSC-derived PLCG2-P522R microglia exhibit an increased induction of major histocompatibility complex (MHC) class II antigen presentation pathways in both AD and WT chimeric mice in vivo. ScRNA-seq fur-

RESEARCH IN CONTEXT

1. **Systematic review**: The authors reviewed the literature using PubMed. Current literature describes the PLCG2 missense variant P522R, primarily expressed by microglia in the brain, is associated with a reduced risk of developing late-onset Alzheimer's disease (AD). Publications in cultured microglia and wild-type P522R knock-in mice revealed this variant has a hypermorphic effect on enzyme activity, triggering calcium store release and microglia activation.

2. **Interpretation**: Our findings in chimeric AD mice demonstrate for the first time that the PLCG2-P522R variant increases the capacity of human microglia to present antigens, a microglial state which has recently been shown to be reduced in AD patient brains, indicating the protective nature of this variant. Moreover, we revealed increased recruitment of CD8+ T cells in a P522R KI 5X mouse model.

3. **Future directions**: The findings on this protective P522R variant implicate the importance of crosstalk between microglia and T cells in AD and the need to further study their interactions in in vivo models and more advanced in vitro models, which might hold great clinical value.

HIGHLIGHT

- PLCG2-P522R and WT human microglia were studied in a chimeric AD mouse model
- The AD-protective P522R variant increased antigen presentation genes in human microglia
- P522R KI 5X mice revealed increased recruitment of CD8+ T cells

ther revealed more P522R-xMGs within the cytokine cluster, which included chemokines involved in the recruitment of T cells to the central nervous system (CNS). Both scRNA-seq and bulk RNA sequencing uncovered a significant increase in the levels of multiple *HLA* genes (MHC class I and II) in P522R xMGs relative to WT xMGs, along with a significant increase in the expression of the transcription factor CIITA, which acts as a master regulator for the expression of MHC class II genes and is also capable of inducing MHC class I genes.[15,16]

Histological analyses of transplanted brains confirmed the increased expression of human leukocyte antigen (HLA)-DR proteins by amyloid plaque-associated xMGs, with no differences in the total number of xMGs surrounding plaques. Therefore, we wondered how increased expression of HLAs by P522R xMGs might affect the progression of AD. HLA genes are expressed by antigen presenting cells and the three loci DR, DQ, and DP encode the major expressed

products of the human MHC class II region. MHC class II molecules bind intracellularly processed peptides, present them to T-helper cells, and have a critical role in the initiation of the adaptive immune response.[17] Interestingly, a similar subset of MHC class II HLA genes was recently shown to be reduced in microglia from human AD brains.[18] Moreover, HLA-DRB polymorphisms are associated with increased risk of AD[2,19,20] and a recent study found that 5XFAD mice that lack MHC class II expression exhibit increased amyloid pathology,[21] further implicating the importance of optimal antigen presentation. Nevertheless, subsequent histological analyses of total plaque burden, amyloid engulfment, and microglial morphology in 5X mice transplanted with P522R versus WT xMGs did not reveal any significant changes. In addition, we observed no increase in the number of reactive GFAP+ astrocytes near P522R versus WT xMGs or amyloid plaques, nor an increase in GFAP protein expression.

In this respect, as our work was carried out using immunodeficient AD mice, a limitation of our model is the lack of T cells, which might clarify why despite increased HLA expression by P522R-xMGs, we were unable to detect differences in AD pathology. As our findings strongly suggest the P522R mutation enhances the crosstalk between innate and adaptive immunity, we obtained brain sections from a recently generated immune-intact PLCG2-P522R KI 5XFAD mouse model. Histological analyses revealed a significant increase in the number of CD8+ T cells, but not CD4+ T cells, within the brains of P522R KI 5XFAD mice compared to WT 5XFAD mice, with T cells often observed in close proximity to microglia. Future studies will be needed to determine whether the larger number of CD8+ T cells includes cytotoxic CD8+ T cells or memory CD8+ T cells, which can restrain certain types of immune response,[22,23] and whether the heightened T cell response induced by the P522R protective variant might provide a surprisingly neuroprotective function. Interestingly, CD8+ T cells are also elevated in human AD brains, can be found closely localized to microglia,[24] and interferon gamma (IFN-y) from memory CD8+ T cells upregulates MHC class II in microglia and keeps them in an activated state.[25] Moreover, despite no significant changes in the number of CD4+ T cells in P522R KI 5X mice, increased crosstalk of P522R microglia with CD4+ T cells might still occur due to increased microglial MHC class II expression, resulting in CD4+ T cell induction of protective autoantibodies or T regulatory cell activity,[26] which could potentially underlie the protective effect of the PLCG2-P522R mutation in AD.[6] Future experiments should address whether P522R mutant microglia have an increased capacity to present antigens to T cells, study how they prime T cells, or whether they aid in T cell-mediated amyloid clearance, through use of P522R KI 5X mice and more advanced in vitro and chimeric models. Moreover, as the P522R mutation increases TREM2 downstream signaling, it will be of great interest to determine whether TREM2 stimulating antibodies,[27,28] such as AL002 currently in a Phase 2 clinical study, could in turn affect microglia–T cell crosstalk and exert similar protection in AD patients as the P522R variant. It is also important to consider the implications of other immune cells, as PLCG2 is also required for the function of B cells, natural killer (NK) cells, mast cells, and to a lesser extent T cells,[29] and thus the P522R mutation could directly as well as indirectly (microglia-mediated) impact the adaptive immune response in AD. Hence, to learn more about the T cell populations, isolation of T cells from brains of P522R KI 5X mice will be needed to collect transcriptomic and proteomic data, as they present a relatively small number of cells within the brain.

Altogether, our novel data on the AD protective PLCG2-P522R variant in chimeric AD mice revealed more P522R-xMGs within the cytokine cluster, including increased expression of chemokines involved in the recruitment of T cells, and increased expression of multiple HLA genes important for antigen presentation, implicating the importance of the crosstalk between microglia and T cells in AD. This observation was further confirmed in P522R KI 5XFAD mice, which revealed an increase in recruitment of CD8+ T cells to the brain. Precisely how these changes reduce AD risk remains unclear. However, the current findings strongly implicate increased microglia–T cell crosstalk, providing the first clues about the protective nature of the P522R variant. These results should therefore inform the design and pursuit of future studies that will further define the precise mechanisms by which microglia and T cells interact to modulate AD progression. In this respect, by using both traditional and chimeric mouse models, the current study provides evidence that the P522R PLCG2 mutation increases the capacity of microglia to recruit and interact with T cells. However, additional studies will be needed to determine whether this protective allele produces a similar response in human subjects. The examination of microglia within human tissue typically requires analysis of *post mortem* samples. Progress has indeed been made with such studies,[18] yet it remains unclear whether agonal state or common comorbidities such as pneumonia may impact the transcriptome of microglia. Fortunately, recent advances in the isolation and examination of T cells from patient-derived cerebrospinal fluid[23] should enable further studies to determine whether PLCG2 mutations similarly impact the recruitment, subtypes, and activation state of CNS-infiltrating T cells in human subjects. Such studies will be critically important to determine the degree to which our initial findings will translate to human clinical application.

2 | CONSOLIDATED RESULTS AND STUDY DESIGN

Chimeric AD and WT mice were generated by transplanting PLCG2-P522R or isogenic WT human iPSC-microglia. Xenografted human iPSC-derived microglia (xMGs) matured and remained within male recipient brains for 7 months, until they were isolated for scRNA-seq and bulk RNA sequencing, and half brains were used for histological analyses. Interestingly, histological analyses of transplanted brains revealed increased expression of HLA-DR proteins by amyloid plaque-associated xMGs, with no differences in the total number of xMGs surrounding plaques. In accordance with our histological observations, both scRNA-seq and bulk RNA seq uncovered a similar significant increase in the levels of multiple HLA genes (MHC class I and II) and revealed an induction of antigen presentation pathways in P522R xMGs relative to WT xMGs. In this respect, a recent study in AD patient and control brains revealed a substantial reduction of the microglial

cluster expressing MHC class II antigen presentation-associated genes in AD patient brains.[18] Thus, in light of our findings this might suggest the protective nature of the P522R variant is related to the induction of MHC class II antigen-presentation genes and pathways in P522R xMGs. Furthermore, our scRNA-seq results also demonstrated an increased expression of chemokines involved in the recruitment of T cells to the CNS. Thus, our findings strongly suggest the P522R mutation enhances the crosstalk between microglia and T cells. To address this fascinating finding and shed light on the crosstalk between P522R microglia and T cells, we had to design an immune-intact PLCG2-P522R KI 5XFAD mouse model, as indeed our chimeric AD mice are immunodeficient. Moreover, histological analyses of amyloid pathology in our chimeric AD mice, including total plaque burden, amyloid engulfment, and microglial morphology in 5X mice transplanted with P522R versus WT xMGs did not reveal any significant changes, which might again be explained by the lack of T cells. Importantly, we obtained brain sections from a recently generated immune-intact PLCG2-P522R KI 5XFAD mouse model and results revealed a significant increase in the number of CD8$^+$ T cells within the brains of P522R KI 5XFAD mice compared to WT 5XFAD mice, with T cells often observed in close proximity to microglia. Altogether, the current findings strongly implicate increased microglia–T cell crosstalk, providing the first clues about the protective nature of the P522R variant, and delivering important information for the design of future studies to address the precise mechanisms by which microglia and T cells interact to modulate AD progression.

3 | DETAILED METHODS AND RESULTS

3.1 | Detailed methods

3.1.1 | Contact for reagent and resource sharing

Further information and requests for resources and reagents should be directed to Mathew Blurton-Jones (mblurton@uci.edu).

3.1.2 | Generation and maintenance of isogenic iPSC lines

The red fluorescent protein (RFP)-α-tubulin expressing iPSC line (AICS-0031-035) was purchased from Coriell. We then used CRISPR-Cas9 modification to introduce the PLCG2-P522R homozygous mutation into the AICS-0035 RFP line (Figure S1A-B in supporting information). Detailed methods of our standard ribonucleoprotein (RNP) CRISPR protocol, quality control, and maintenance of all iPSC lines can be found in McQuade et al.[30] iPSC lines were used under approved human Stem Cell Research Oversight (hSCRO) committee protocols.

Materials used include (1) gRNA 5′ CCCAAAATGTAGTTCTGTAG; (2) the ssODN template 5′ tcgtcctcttctccaccttcttgtggaaccatttctccccaa-aatgCagCtctgtagggCgGatatcctgggccgcaaagagaggagggggtttctgaaagcct-tggacca; (3) and the following primers to assess candidate

clones and confirm the absence of off-target effects: PLCG2_F: accgttcactgcatgtctca; PLCG2_R:cctgagctagaaccactcgc; PLGM2L1_F: gttgtgtgcatgtagtggcag; PLCG2L1_R:tacatttcttcagaaggaccaggaa.

3.1.3 | iPSC-derived hematopoietic progenitors and microglia differentiation

HPCs and iMGs were differentiated as detailed in a well-established protocol.[13]

3.1.4 | Animals

All animal procedures were conducted in accordance with National Institutes of Health guidelines and the University of California, Irvine Institutional Animal Care and Use Committee. M-CSFh mouse line (hCSF1) was purchased form Jackson Laboratories (stock #017708) and contains Rag2 and Il2rγ deletions and humanized M-CSF, which is necessary for human microglial engraftment. The 5XFAD-hCSF1 (5X-hCSF1) model was created by backcrossing the M-CSFh mouse with the well-established 5XFAD transgenic model, which overexpresses co-integrated transgenes for familial Alzheimer's disease (FAD) mutant APP (Swedish, Florida, and London) and mutant PS1 (M146L and L286V).[31] ScRNA seq results were obtained from WT and P522R xMGs isolated from hCSF1 5X and WT chimeric mice. To confirm and further extend our analysis via bulk RNA sequencing of WT and P522R xMGs, a second cohort of age- and sex-matched 5X-MITRG chimeric mice was used. MITRG mice were derived from the M-CSFh parental line via the inclusion of two additional humanized alleles—GM-hCSF/CSF2 and hTPO (Thrombopoietin), purchased from Jackson Laboratories—and backcrossed with 5XFAD mice. We recently confirmed that MITRG and hCSF1 mice enable equivalent engraftment and survival of human iPSC-derived microglia as the presence of the humanized CSF1 allele is necessary whereas inclusion of the CSF2 and TPO alleles are dispensable.[14] As expected, immunohistological analyses of P522R versus WT xMGs showed similar trends in both mouse cohorts; thus, histological data was pooled. Age-matched male mice were used and group housed on a 12 hour/12 hour light/dark cycle with food and water ad libitum.

P522R KI 5XFAD mice used for histological analyses were generated by IU/JAX/UCI MODEL-AD consortium (JAX MMRRC Stock #029598; https://www.model-ad.org/strain-table/). P522R KI mice were generated by using CRISPR/Cas9 endonuclease-mediated genome editing to introduce a single nucleotide change at c.1565 C > G (p. P522R), which models a human single nucleotide polymorphism. These mice were maintained on the B6 background and crossed with 5XFAD mice (JAX MMRRC Stock #034848) to yield P522R KI 5XFAD mice. We used 7.5-month-old male mice in the current study. Up to five mice were housed per cage with SaniChip bedding and LabDiet® 5K52/5K67 (6% fat) feed. The colony room was kept on a 12:12 hour light/dark schedule with the lights on from 7:00 am to 7:00 pm daily. The mice were bred and housed in specific

pathogen-free conditions. Animals used in the study were housed in the Stark Neurosciences Research Institute Laboratory Animal Resource Center, Indiana University School of Medicine, and all experimental procedures were approved by the Institutional Animal Care and Use Committee (IACUC).

3.1.5 | Postnatal intracerebroventricular transplantation of HPCs

P2 to P3 WT and 5X-hCSF1/MITRG were placed in a clean cage over a heating pad with a nestlet from the home cage to maintain the mother's scent. Male pups were then placed on ice for 2 to 3 minutes to induce hypothermic anesthesia. Free-hand transplantation was performed using a 30-gauge needle affixed to a 10 μL Hamilton syringe; mice received 1 μL of HPCs suspended in sterile 1X Dulbecco's phosphate-buffered saline (DPBS) at 50K cells/μL at each injection site (eight sites) totaling 400K cells/pup. For further details and validation of this chimeric approach please see Hasselmann et al.[14]

3.1.6 | Immunohistochemistry

At 7 months of age, mice were sacrificed by intracardiac perfusion of phosphate-buffered saline (PBS) and brains rapidly removed and hemisected along the midsagittal plane. Half brains were then processed for human microglial isolation (see below) and the other half was drop fixed in 4% (w/v) paraformaldehyde for 48 hours. Fixed brains were subsequently cryoprotected in 30% sucrose, sectioned coronally into 40 μm-thick slices on a freezing microtome, and stored at 4°C in PBS with 0.05% NaN3 in PBS. For immunofluorescent staining, free-floating sections were blocked for 1 hour in PBS, 0.2% Triton X-100, and 10% goat serum. Sections were then placed in primary antibodies diluted in PBS and 1% goat serum and incubated overnight at 4°C. Samples were rinsed three times, incubated in Alexa fluorophore-conjugated secondary antibodies for 1 hour, rinsed again, and mounted on slides. Sections were labeled with combinations of Amylo-Glo RTD Amyloid Plaque Stain Reagent (1:100; Biosensis TR-300-AG; incubation for 20 minutes prior to the addition of the primary antibodies), anti-TagRFP (1:10,000; Kerafast EMU113), anti-HLA-DRB1 (1:200; Invitrogen 14-9956-82), anti-CD9 (1:200; HI9a, BioLegend 312102), anti-apolipoprotein E (*APOE*; 1:1000, Thermo Fisher PA5-27088), anti-Ku80 (1:200; Abcam ab79220), anti-LAMP1 (1:200; Abcam ab25245), anti-GFAP (1:2000, Abcam ab4674), anti-Iba1 (1:200; Wako 019-19741), anti-CD8 (1:250, Invitrogen 14-0081-82) and anti-CD4 (1:250, BioLegend 100506).

3.1.7 | Confocal microscopy and immunohistochemistry quantification

Immunofluorescent sections were visualized and captured by a blinded observer using an Olympus FV3000RS confocal microscope. Images represent confocal Z-stack (five images per mouse) taken within the retrosplenial granular cortex and piriform cortex at 40x magnification with identical laser and detection settings between genotypes. Human microglia were detected and quantified through RFP immunofluorescence within 10 μm per plaque (Amylo-Glo, blue) using the Cellsense software on the Olympus FV3000. Plaques near the borders of the image were excluded, and for plaques within 10 μm of each other, only the plaque with the highest number of xMGs was examined (Welch's *t*-test). IMARIS-based quantification of HLA-DR, CD9, APOE, LAMP1, GFAP, and total plaque load was performed using the "Surfaces" function and were measured by the sum of surfaces for each image. Mean intensity of GFAP surfaces was analyzed by Imaris. To assess the amyloid plaque phagocytotic characteristics of RFP⁺ xMGs, Imaris software Cell Detection feature was used. Internalized Amylo-Glo⁺ vesicle number and area were calculated within RFP⁺ xMGs. Confocal stitch images were taken to quantify the overall plaque load between the groups using Amylo-Glo labeling. By analyzing particle features on ImageJ Fiji software we were able to quantify size, number, and %area of the plaques (total plaque load) in both cortex and hippocampus. Mice that received unilateral injection (left side) were examined to analyze the Amylo-Glo⁺ plaque load in the transplanted versus untransplanted hemisphere of AD chimeric mice (n = 3 mice). 10X stitch confocal images were taken from left and right hemispheres. Number of Ku80⁺ spots (marker for human nuclei, human xMGs) and Amylo-Glo⁺ surfaces were calculated using Imaris software. Microglia morphology was analyzed by detecting RFP⁺ xMGs using the Filament feature in Imaris software. As expected, immunohistological analyses of P522R versus WT xMGs showed similar trends in both mouse cohorts, thus histological data was pooled (n = 10 [4 hCSF1 and 6 MITRG] mice for P522R xMGs and n = 7 mice [4 hCSF1 and 3 MITRG] for WT xMGs in AD chimeric mice; n = 7 [3 hCSF1 and 4 MITRG] mice for P522R xMGs and n = 7 mice [3 hCSF1 and 4 MITRG] for WT xMGs in WT chimeric mice). To analyze the number of mouse T cells in the dorsal subiculum of brain sections from PLCG2-P522R KI and PLCG2-WT 5X mice, images were taken at 20X and Imaris software was used to quantify total sum of plaque area (Amylo-Glo) and number of CD8⁺ and CD4⁺ spots were counted.

3.1.8 | Ratiometric calcium imaging

Ratiometric Ca^{2+} imaging using Fluo-4 and Fura-red was done as described previously.[30] Briefly, human iPSC-derived RFP-expressing iMGs were plated on fibronectin-coated glass bottom dishes (MatTek Corporation). Twenty-four hours later, cells were loaded with 3 μM Fluo-4 AM and 3 μM Fura-Red AM (Molecular Probes) in the presence of Pluronic Acid F-127 (1:1000, Molecular Probes) for 30 minutes at room temperature (RT). After dye washout, cells were bathed in 1 mM Ca^{2+} Ringer's solution. Time-lapse videos were acquired on the Olympus Fluoview FV3000i confocal LSM equipped with high speed resonance scanner, IX3-ZDC2 Z-drift compensator and 40X silicone oil objective (NA 1.25), at RT and at 20 frames/minute. Fluo-4 and Fura-red were excited using a 488 nm diode laser (0.05% laser

transmissivity, 10% laser ND filter) and emitted light was collected using high-sensitivity cooled GaAsP photomultiplier tubes set to wavelengths 494 to 544 and 580 to 680 nm, respectively. There was negligible bleed-through of RFP into the red (Fura-Red) channel with the 488 nm laser. ER Ca^{2+} store was depleted with 2μM thapsigargin (TG) in Ca^{2+} free Ringer's solution and 1 mM Ca^{2+} was added back to induce SOCE. Videos were exported to Image J as tiff files, background subtracted, and single-cell analysis was done by drawing regions of interest (ROIs) around each cell in the imaging field. Average intensities in the green and red channels were calculated for each ROI at each timepoint and Fluo-4/Fura-Red ratio was obtained to generate traces reflecting single-cell and average changes in cytosolic Ca^{2+} over time. Single-cell baseline cytosolic Ca^{2+} level was calculated with cells resting in 1 mM extracellular Ca^{2+}. The ER store-content was determined by quantifying the cumulative cytosolic Ca^{2+} levels at the single-cell level as area under the curve (AUC) after TG-induced store-release. AUC was calculated by the trapezoid method. Rate of SOCE was calculated at the single-cell level as the slope of cytosolic Ca^{2+} rise after the re-addition of 1 mM Ca^{2+} after ER store-release.

3.1.9 | Tissue dissociation for single-cell and bulk RNA sequencing

All steps were performed on ice or at 4°C with ice-cold reagents and all centrifuge steps were performed for 10 minutes at 400 x g with full brake and acceleration unless otherwise stated. Anesthetized mice were intracardially perfused with 1X DPBS, half brains were dissected, the cerebellum was removed, and tissue was stored in RPMI 1640 until subsequent perfusions were completed. Brains were manually homogenized using a 7 mL Dounce homogenizer by adding 4 mL of RPMI 1640 and performing 10 strokes with the "loose" pestle followed by 10 strokes with the "tight" pestle. Samples were then run through a pre-soaked 70uM filter and the filter was washed with 10 mL of RPMI 1640. The sample was pelleted by centrifugation and myelin was removed by resuspension in 30% Percoll overlaid with 2 mL of 1X DPBS centrifuged at 400 x g for 20 minutes with acceleration and brake set to 0. The myelin band and supernatant were discarded and cell pellets were resuspended in 80 μL MACS buffer (0.5% bovine serum albumin [BSA] in 1X DPBS) + 20 μL Mouse Cell Removal beads (Miltenyi) and incubated at 4°C for 15 minutes. Magnetically labeled mouse cells were separated using LS columns and the MidiMACs separator (Miltenyi) while the unlabeled human cells were collected in the flowthrough. Human cells were then pelleted by centrifugation and dead cells were magnetically removed using the Dead Cell Removal kit, Annexin V (Stem Cell Technologies) by resuspending the pellets in 100 μL of buffer (2% BSA + 1 mM CaCl2 in 1X PBS) in 5 mL polystyrene round-bottom tubes and following manufacturer's protocol. Live cells were centrifuged, resuspended in 50 to 100 μL of MACS buffer, and concentrations were determined by counting on a hemocytometer. For scRNA-seq final cell concentrations were then adjusted to 900 to 1000 cells/μL. Bulk RNA sequencing samples were stored at –80°C before proceeding to RNA isolation.

ScRNA-seq was performed on 7-month-old male hCSF1s: n = 2 5X mice with WT xMGs, n = 1 5X mouse with P522R xMGs; n = 1 WT mouse with WT xMGs, n = 1 WT mouse with P522R xMGs. To confirm and further extend our analysis in a larger cohort via bulk RNA sequencing of WT and P522R xMGs, a second cohort of age and sex-matched 5X-MITRG chimeric mice was used. We recently confirmed that MITRG and hCSF1 mice enable equivalent engraftment and survival of human iPSC-derived microglia as the presence of the humanized CSF1 allele is necessary whereas inclusion of the CSF2 and TPO alleles are dispensable.[14] As expected, altered genes remained consistent between single-cell and bulk RNA seq and strengthened our single-cell observations. Mice used for bulk RNA sequencing include 7-month-old male MITRGs: n = 3 5X mice with WT xMGs, n = 6 5X mice with P522R xMGs; n = 3 WT mice with WT xMGs, n = 7 WT mice with P522R xMGs.

3.1.10 | scRNA library preparation and sequencing

scRNA-seq library preparation was performed according to the 10X Genomics Chromium Single-cell 3′ Reagents kit v3 user guide except that sample volumes containing 25,000 cells were loaded onto the 10X Genomics flow cell to capture ≈10,000 total cells. The 10X Genomics workflow was then followed according to the manufacturer's protocol and libraries were pooled at equimolar concentrations for sequencing on an Illumina NovaSeq 6000, targeting ≈50,000 reads per cell. Reads were aligned to the human GRCH38 transcriptome (CellRanger release 3.0.0) using CellRanger 3.1.0 (10X Genomics).

3.1.11 | scRNA data visualization and differential gene analysis

Filtered feature-barcode matrices were imported into Seurat v3[32] for further processing. Cells were filtered out by mitochondrial gene content (> 10%), ribosomal content (> 25%), number of total features (< 1000 or > 2500), unique molecular identifier (UMI) count (< 1000 or > 4500), and cell cycle gene content (gene module score > 0). Filtered samples were normalized using SCTransform, using UMI count, percent ribosomal, and percent mitochondrial features as regression variables. Samples from WT or 5X mice were combined into an integrated dataset using 2000 features for integration. Principal component analysis (PCA) was performed on integrated data, and an elbow plot was used to select the number of principal components (PCs) to use for clustering. Clustering was performed using two PC cutoffs (12, 16) and a range of resolution parameters (0.1 to 1.2); after examining differentially expressed genes among the clusters for each parameter set, a PC cutoff of 12 and a clustering resolution of 0.3 were selected for further analysis, as they provided the most biologically consistent representation of the data. UMAP dimensional reduction was performed using the same PC cutoff. Differentially expressed genes among clusters were determined using the Seurat's FindAllMarkers function, using a Wilcoxon rank sum test, a minimum fraction of cells expressing

a gene of 0.25, a log2 fold change cutoff of 0.25, and a maximum adjusted *P*-value of 0.05. Clusters were assigned identities based on manual inspection of differentially expressed genes. Additionally, subsequent analysis identified a small cell population (543 cells; Figure S11 in supporting information) primarily present in only samples from 5X mice, which were removed as the cluster did not appear to be biologically relevant. The y-axis of the violin plots as will be depicted in Figure 2 and Figure S6 feature counts per cell divided by the total counts for the cell and multiplied by a scale factor of 10,000, then natural-log transformed using log1p, using the NormalizeData function in Seurat.

Pseudotime analysis was performed using Monocle 3.[33] Variable features identified for dataset integration and PCA and UMAP embeddings from the Seurat analysis were also used for trajectory analysis. The trajectory graph was constructed using the learn_graph function with default parameters. The starting node for pseudotime ordering was chosen as the graph vertex closest to the set of cells in the homeostatic cluster.

3.1.12 | RNA isolation and bulk sequencing preparation

Total RNA was isolated using RNeasy Mini kit (Qiagen). xMG samples were lysed in $700\,\mu$L RLT buffer and RNA was isolated per the manufacturer's instructions with DNAse treatment (10 minutes, RT). Centrifugation times were increased to $16,000 \times g$ for 1.5 minutes to maximize yield. RNA integrity was measured using the Bioanalyzer Agilent 2100. All libraries were prepared from samples with RNA integrity values ≥ 8.9 (1 sample 8.1) to create RNA-seq libraries through the SMART-seq v4 ultra low input kit. Samples were sequenced on the Illumina NovoSeq 6000.

3.1.13 | Bulk RNA sequencing analysis

RNA sequencing data quality was checked using FastQC 0.11.7 (Babraham Bioinformatics) and trimmed of adapters and low-quality sequence with Trimmomatic 0.35[34] using parameters SLIDINGWINDOW:4:20 LEADING:5 TRAILING:5 MINLEN:30. Remaining reads were aligned to a human reference transcriptome (GRCh38, Ensembl release 88) and abundances were quantified using Kallisto 0.46.1.[35] Differential expression was computed in DESeq2 1.26.0.[36] Genes with fewer than 10 counts across all samples were removed, and a significance cutoff of $P < .05$ was used (Figure S11). Transcription factor binding sites occurring within 500 bp upstream regions of genes were identified using blerr (github.com/englandwe/blerr), using the JASPAR 2018 set of transcription factor binding sites[37] and a Z-score significance cutoff of two. Overrepresented GO terms were identified using PANTHER[38] with a maximum false discovery rate—adjusted *P*-value of .05 and visualized as networks using the EnrichmentMap plugin for Cytoscape 3.7.2.[39,40] Plots were generated using ggplot2 3.3.2,[41] pheatmap 1.0.12 (https://CRAN.R-project.org/package = pheatmap), and Vennerable 3.1.0.9000 (https://rdrr.io/rforge/Vennerable).

3.1.14 | Statistical analysis

All statistical analysis were performed using either R 3.6.2 (https://www.R-project.org/, R Foundation for Statistical Computing) or Prism 8 (Welch's t-test and non-parametric Mann-Whitney U-test).

3.2 | Detailed results

3.2.1 | The protective P522R variant of PLCG2 increases HLA-DR expression in plaque-associated xMGs in chimeric AD mice but has no effect on microglial plaque proximity

After confirmation that introduction of the P522R mutation produces a hypermorphic effect on calcium signaling in iMGs (Figure S2A-F in supporting information), HPCs were transplanted into our recently described WT and AD chimeric mouse models.[14] As PLCG2 signals downstream of TREM2, which is crucial for the formation of disease-associated microglia (DAMs),[42] we first examined the effect of the P522R variant on the plaque-associated DAM subpopulation. Our results revealed that P522R xMGs significantly increase expression of HLA-DR protein, which remains elevated when further normalized to plaque load. In contrast, no differences in the number of xMGs within $10\,\mu$m of fibrillar amyloid plaques or total plaque area were observed between P522R xMGs and WT xMGs (Figure 1A-F, Figure S3 in supporting information). In addition, no difference in the DAM-specific markers CD9 (Figure 1G-K) or human-specific APOE (Figure S4A-E in supporting information), were detected relative to WT xMGs. Accordingly, there was also no change in the amount of LAMP1 immunoreactive dystrophic neurites around plaques (Figure S4F). In WT chimeric mice, P522R xMGs showed a similar, albeit a non-significant, trend toward increased HLA-DR immunoreactivity (Figure S5A-C in supporting information). Overall, these results indicate the PLCG2-P522R variant increases HLA-DR expression by plaque-associated xMGs, without altering the proximity of microglia to plaques.

3.2.2 | The PLCG2-P522R variant increases the number of xMGs within the cytokine cluster by scRNA-seq and elevates microglial expression of multiple HLA and chemokine genes in AD chimeric mice

Seven months after transplantation, xMGs were isolated from 5X and WT brains and examined by 10X scRNA-seq. Analysis revealed six discrete clusters of xMGs, each representing a unique microglial state (Figure 2A-C). To determine whether the P522R mutation induces a shift in these populations, we next performed differential proportion analysis (DPA),[43] revealing a significant reduction in homeostatic microglia in P522R mice ($P = .011$), accompanied by an increase in cytokine-expressing microglia ($P = .001$) and a trend toward increased interferon-responsive microglia ($P = .08$; Figure 2D). Interestingly, we also observed a significant increase of many genes (adj-$P < .05$) within each cluster, including cytokine and chemokine genes (CCL2, CCL3,
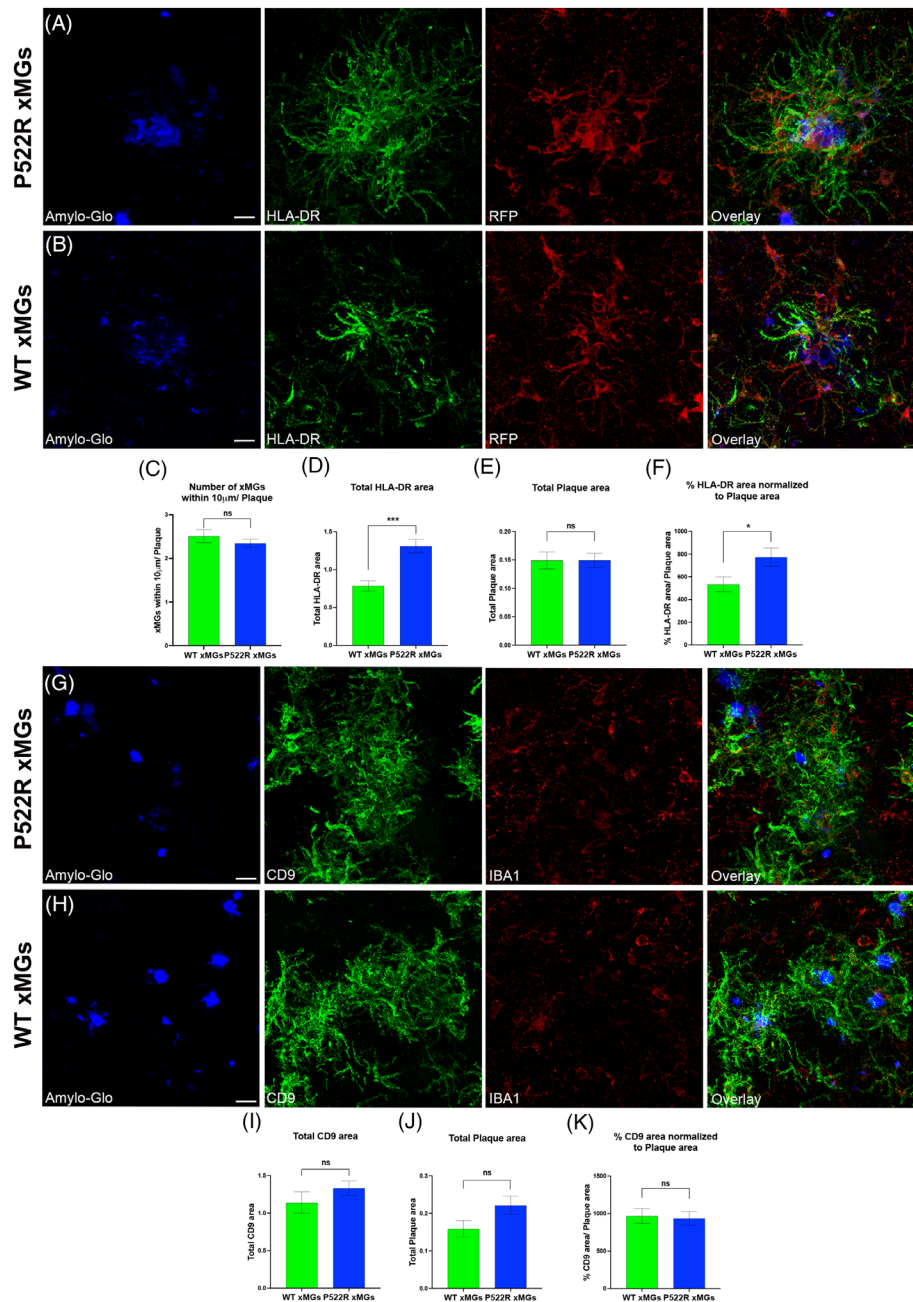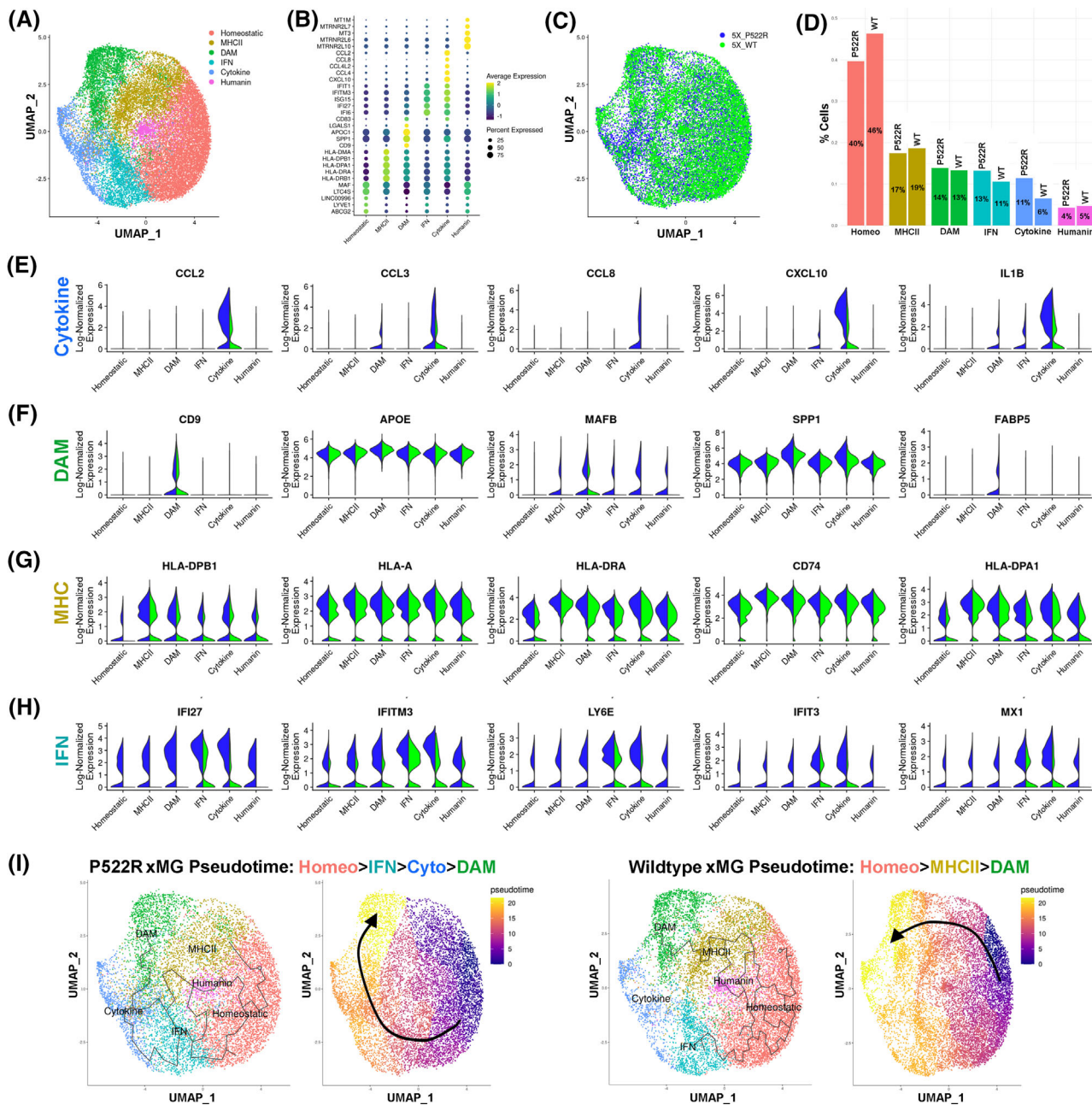
FIGURE 1 P522R xenografted human induced pluripotent stem cell—derived microglia (xMGs) exhibit increased human leukocyte antigen (HLA)-DR protein levels around plaques, with no changes in CD9 or microglial plaque proximity. Quantification of the proximity of xMGs to amyloid plaques (blue, Amylo-glo) in 7-month-old chimeric Alzheimer's disease mice revealed no changes in plaque-associated red fluorescent protein (RFP) P522R-PLCG2 xMGs (A) versus RFP PLCG2-WT xMGs (B) within a 10 μm radius of the outer border of plaques ($P = .37$) (C). A significant increase in total levels of HLA-DR was detected (D), without a significant difference in total plaque load ($P = .98$) (E). A significant increase of the percentage of HLA-DR area normalized to plaque area (F) was also observed in P522R xMGs versus WT xMGs. No changes in total levels of the disease-associated microglia marker CD9 ($P = .29$), total plaque area ($P = .076$), or percentage of CD9 normalized to plaque area ($P = .80$) were detected in mutant xMGs relative to WT (G-K); Welch's t-test *$P < .05$; ***$P < .001$; n = 7 mice WT xMGs, n = 10 mice P522R xMGs; five images per mouse; Confocal images A–B scale of 10 μm, G–H scale of 15 μm

CCL8, CXCL10, IL1B; Figure 2E) and several DAM genes (MAFB, SPP1, and FABP5; Figure 2F), although no significant increase in CD9 and APOE mRNA was detected consistent with our histological findings. We also observed a striking increase of multiple genes belonging to the HLA gene complex, including HLA-DPB1, HLA-A, HLA-DRA, CD74,

and HLA-DPA1, which was observed across multiple scSeq clusters (Figure 2G) and in agreement with our histological observations of HLA-DR. In addition, we observed increased expression of several IFN genes including IFI27, IFITM3, LY6E, IFIT3, and MX1 (Figure 2H). In this respect, pseudotime analysis revealed the P522R mutation alters the

FIGURE 2 Single-cell RNA sequencing (scRNA-seq) reveals a significant increase in the cytokine cluster, induction of human leukocyte antigen (HLA) genes and an altered activation trajectory for PLCG2-P522R xenografted human induced pluripotent stem cell–derived microglia (xMGs). UMAP dimension reduction reveals six distinct clusters of human microglia in chimeric Alzheimer's disease mice (A). A dot plot reveals top marker genes for each of the six clusters (false discovery rate–adjusted *P*-value < .05). Size of the circles indicate the percentage of cells expressing that gene and color indicates average expression levels (B). UMAP depiction of P522R microglia (blue) and wild-type (WT) microglia (green) demonstrate distributions of both mutant and WT cells within each cluster (C). The P522R mutation elicits a significant reduction in the number of homeostatic microglia (*P* = .011), an increased trend of cells in the interferon (IFN) cluster (*P* = .08), and a significant increase of P522R xMGs within the cytokine cluster (*P* = .001) analyzed through DPA (Figure S11) (D). Violin plots highlighting cytokine (E), disease-associated microglia (DAM) (F), major histocompatibility complex (MHC; G), and IFN (H) genes that are significantly enriched within several clusters within PLCG2-P522R microglia (Figure S11). Pseudotime analysis was performed to predict the trajectory by which P522R and WT human microglia transition toward a DAM phenotype (I). Surprisingly, two different trajectories were observed; whereas P522R xMGs transition toward the DAM phenotype via heightened IFN responsive gene expression followed by cytokine and chemokine induction, WT xMGs take a more direct path from homeostatic to MHC class II to DAM
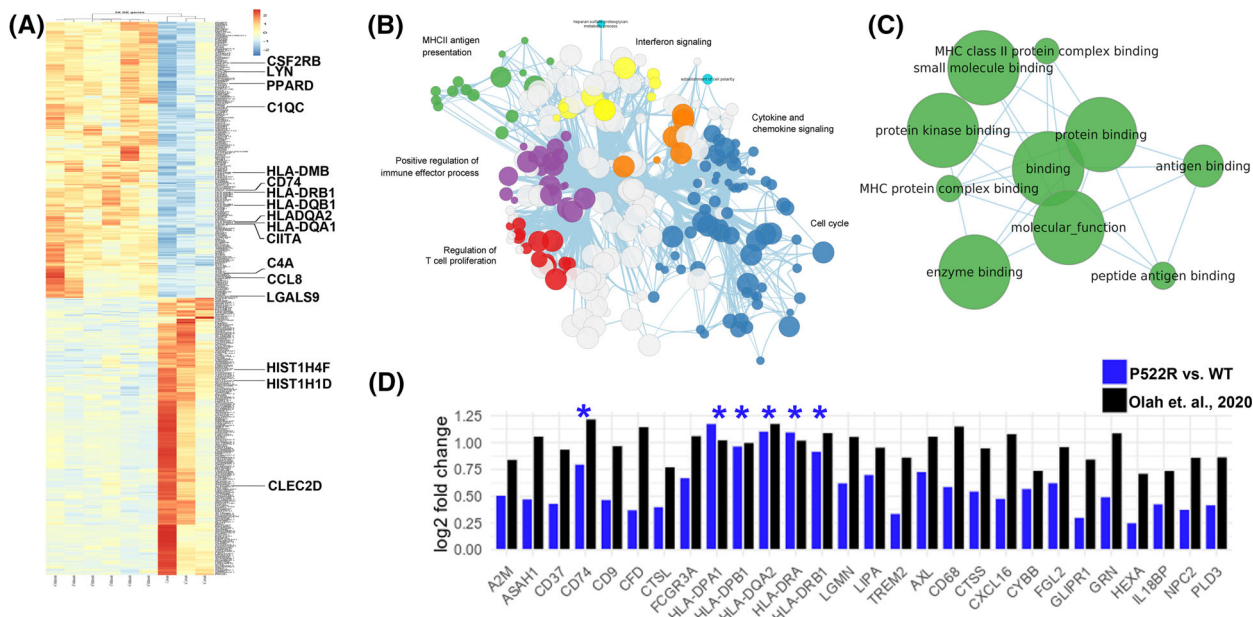
FIGURE 3 Bulk RNA sequencing (RNA-seq) demonstrates the consistent induction of antigen presentation genes by P522R xenografted human induced pluripotent stem cell—derived microglia (xMGs), that are reduced by microglia in human Alzheimer's disease (AD) brains. Human microglia were isolated from a second cohort of chimeric AD mice and examined by bulk RNA-seq, revealing a total of 505 differentially expressed genes (DEGs) with a log2 fold change of > 1 and false discovery rate < 0.05 (A) (Figure S11). Consistent with the single-cell RNA sequencing (scRNA-seq) results, many human leukocyte antigen (HLA)-associated genes were strongly upregulated in P522R microglia including CD74, HLA-DRB1, and CIITA, the primary transcription factor that regulates MHC class II gene expression. Next, Gene Ontology analysis was performed to identify biological processes that are enriched in P522R microglia (B). This analysis confirmed the strong induction of MHC class II and antigen presentation pathways, cytokine and chemokine signaling, cell cycle regulation, interferon responsive pathways, and the regulation of T cell proliferation and other immune effector signals. Analysis of molecular functions further emphasized the increase of MHC class II protein binding and antigen binding (C). Interestingly, genes expressed by P522R xMGs in chimeric AD mice overlap with many genes shown to be enriched in a subpopulation of human microglia that is significantly reduced in AD patient brains (Cluster 7,[18] Figure S11) and P522R xMGs significantly upregulate six of these genes (*) that are essential for antigen presentation (D). Thus, the P522R mutation appears to induce a transcriptomic signature in human microglia that is enriched in control patients who have not developed dementia

trajectory of human microglial responses to amyloid by promoting progression through an interferon-responsive pathway toward the DAM phenotype compared to WT xMGs that move toward a DAM signature via an MHC class II intermediate state (Figure 2I). Last, while we did not observe a significant increase of HLA-DR protein levels in P522R xMGs transplanted into WT chimeric mice by immunohistochemistry (IHC; $P = .085$), scRNA-seq of WT chimeric mice revealed elevations in cytokine, DAM, MHC, HLA, and IFN genes, with a significant increase in the proportion of microglia within the cytokine cluster by DPA ($P = .04$; Figure S6A-H in supporting information).

3.2.3 | The P522R variant promotes the expression of antigen presentation genes by xMGs that also define a cluster of microglia that are reduced in human AD

scRNA-seq provides important information about microglial cell states. However, to provide a deeper understanding of the biological pathways that are altered by the PLCG2-P522R mutation, we performed bulk RNA sequencing of WT and P522R xMGs isolated from additional AD chimeric mice. A heatmap comparing samples obtained from

AD mice transplanted with either PLCG2-P522R or PLCG2-WT xMGs revealed significantly upregulated genes in P522R xMGs including CCL8, an array of HLA genes, and CIITA (Figure 3A). Interestingly, CIITA (class II trans-activator) is a master regulator of the expression of HLA genes which encode the MHC class I and II protein complex.[15,16] Gene Ontology analysis of upregulated genes revealed MHC class II antigen presentation as a predominant signal, along with cytokine/chemokine signaling, interferon signaling, and regulation of T cell proliferation. Gene ontology analysis of molecular function further emphasized the increase of MHC class II protein binding and antigen binding (Figure 3B-C). Bulk RNA sequencing of microglia isolated from WT chimeric mice revealed a similar P522R-dependent increase in HLA genes even in the absence of amyloid pathology, suggesting that the P522R mutation likely primes microglia to adopt an MHC class II state (Figure S7A-C in supporting information). Overall, bulk RNA sequencing of isolated xMGs from chimeric AD mice confirmed and extended upon our scRNA-seq findings, further highlighting increased expression of genes and pathways involved in antigen presentation by P522R xMGs.

Interestingly, a recent study identified nine microglial subtypes in AD and control patient brains.[18] Of these, one cluster in particular (cluster 7) is characterized by the expression of CD74 and many other
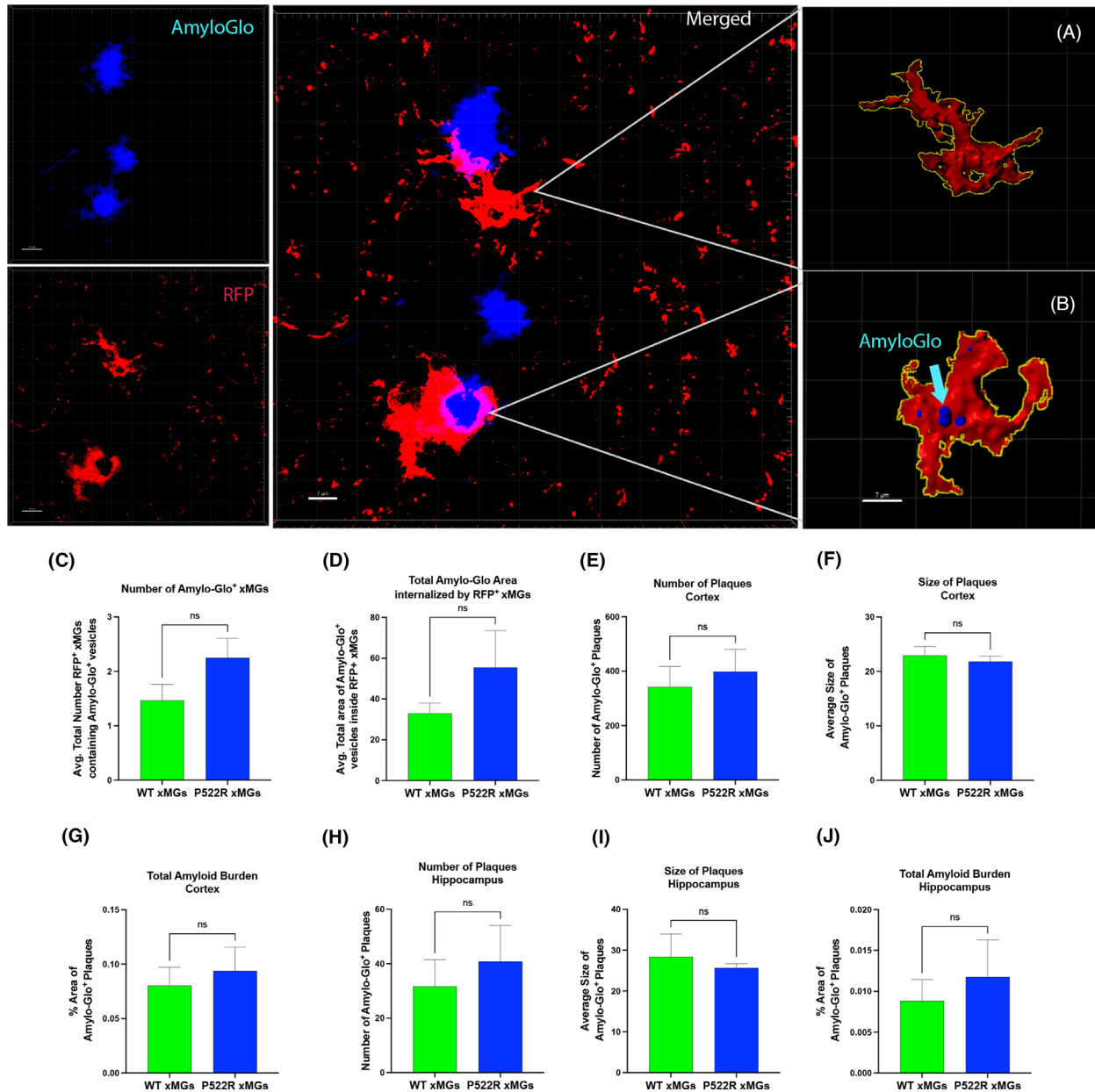
FIGURE 4 The P522R variant did not induce differences in microglial plaque engulfment or total plaque burden. Analysis of fibrillar amyloid (Amylo-Glo, blue) revealed no significant impact of the protective variant on total number of red fluorescent protein (RFP)+ xenografted human induced pluripotent stem cell—derived microglia (xMGs; red) engulfing amyloid ($P = .11$) (**A-C**) or total microglial amyloid internalization ($P = .26$) (**D**). No significant differences were observed in the number ($P = .61$), size ($P = .57$), or total plaque burden ($P = 0.63$) in the entire brain cortex (**E-G**), nor in number ($P = .59$), size ($P = .65$), or total plaque burden ($P = 0.58$) in the hippocampus (**H-J**) of Alzheimer's disease chimeric mice; n = 6 mice for wild-type xMGs, 8 mice for P522R xMGs; 5 images per mouse, scale at 7 μm (A-D); 10X stitch of cortex and hippocampus per mouse (E-J); Welch's t-test $^*P < .05$

MHC class II antigen presentation-associated genes and was shown to be substantially reduced in AD patients.[18] In this respect, our data indicate that many of the genes enriched in P522R xMGs overlap with those in the human AD cluster 7 and are essential for antigen presentation[18] (Figure 3D). Altogether, our data demonstrate that the P522R variant increases the expression of genes important for antigen presentation, which are conversely downregulated in human AD microglia.

3.2.4 | PLCG2-P522R xMG-transplanted AD mice did not reveal a significant increase in microglial plaque internalization, total plaque load, microglial morphology, or astrocyte reactivity

To further examine whether P522R xMGs induce changes in AD plaque pathology, extensive characterization of fibrillar amyloid (Amylo-Glo) was performed. First, we analyzed whether transplantation of xMGs
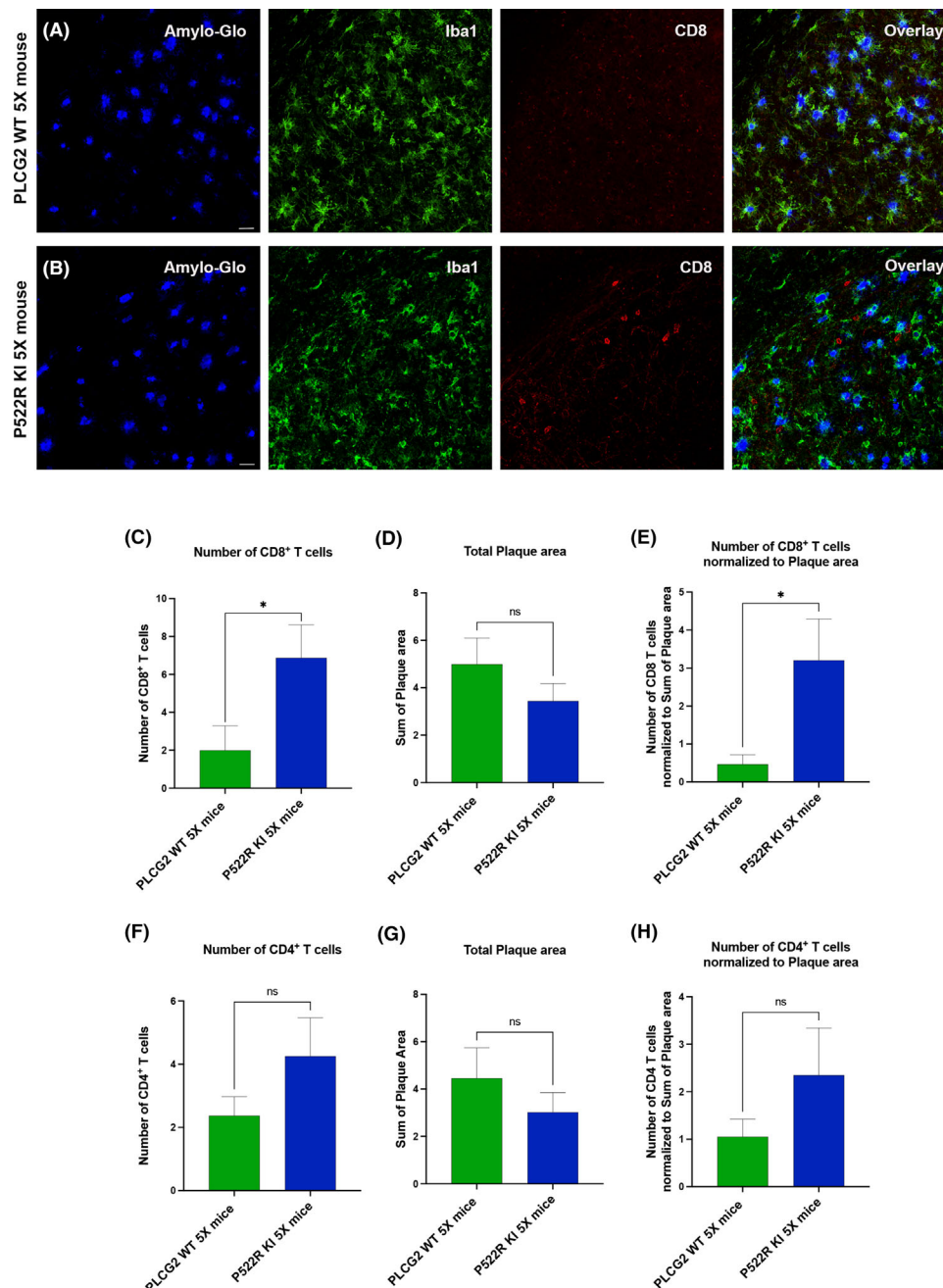
FIGURE 5 Immunocompetent P522R KI 5X mice reveal increased recruitment of CD8+ T cells, but not CD4+ T cells, to the dorsal subiculum. Quantification of the number of CD8+ T cells in the dorsal subiculum of P522R KI 5X mice versus PLCG2-WT 5X mice (Amylo-Glo+ plaques, blue; Iba1+ mouse microglia, green; CD8+ T cells, red) revealed a significant increase in the number of CD8+ T cells, with no difference in total plaque load ($P = .26$) and a significant increase of the number of CD8+ T cells normalized to plaque area (A-E). No significant difference in the number of CD4+ T cells ($P = .19$), total plaque load ($P = .36$), or number of CD4+ T cells normalized to plaque area ($P = .25$) were observed (F-H). C-H Welch's t-test $^*P < .05$; n = 8 mice per genotype; Confocal images at 20X, A-B at a scale of 20 μm

into our AD mouse model affected overall plaque number by performing adult unilateral intrahippocampal transplantations. xMGs were shown to migrate throughout the left hippocampus (in which they were injected), but not the right hippocampus (which received a PBS control injection). xMGs were found surrounding plaques ipsilateral to the injection site, but no effect on total plaque number was observed when comparing plaque load between the ipsilateral and contralateral

hippocampi (Figure S8 in supporting information). Further analyses of plaque load in 5X mice transplanted with P522R versus WT xMGs revealed no significant impact of the protective variant on total number of xMGs engulfing amyloid, total microglial amyloid internalization, nor number, size, or total plaque burden in the cortex and hippocampus of AD chimeric mice (Figure 4A-J). Furthermore, we observed no significant changes in microglial morphology in chimeric AD mice

including branch complexity, volume, diameter, number, and cell body size (Figure S9A-F in supporting information). Last, we analyzed GFAP+ immunoreactive astrocytes, as it was previously reported that P522R KI mice exhibit increased GFAP expression.[11] We did not observe a significant effect on the number of reactive GFAP+ astrocytes near P522R versus WT xMGs, nor an increase in GFAP intensity in both AD and WT chimeric mice, and no significant changes in the number of GFAP+ astrocytes near plaques in AD chimeric mice transplanted with P522R versus WT xMGs (Figure S10A-G in supporting information).

3.2.5 | The P522R variant promotes the recruitment of CD8+ T cells in P522R KI 5X mice

Both histological analyses and RNA sequencing of xMGs in AD chimeric mice strongly suggest the P522R mutation enhances the crosstalk between innate and adaptive immunity. However, to allow engraftment of human xMGs in mouse brains, our mouse model is genetically immunodeficient (Rag2$^{-/-}$, il2r$\gamma^{-/-}$), thereby precluding the examination of T cells in this model. Therefore, we further examined the possible interactions between P522R-microglia and T cells in brain tissue obtained from immune-intact PLCG2-P522R KI 5X mice. Histological analyses revealed a significant increase in the number of CD8+ T cells, but not CD4+ T cells, in PLCG2-P522R KI versus PLCG2-WT 5X mice and T cells were frequently observed in close proximity to microglia (Figure 5A-H). Overall, these results show that the protective P522R-PLCG2 variant significantly increases the recruitment of CD8+ T cells to the brain and potentially increases the interaction between microglia and CD4+ T cells via increased MHC class II expression.

CONFLICT OF INTEREST

M.B.J. is a co-inventor of patent application WO/2018/160496, related to the differentiation of pluripotent stem cells into microglia and co-founder of NovoGlia Inc.

ORCID

Christel Claes https://orcid.org/0000-0002-7765-0445

REFERENCES

1. Shen L, Jia J. An Overview of Genome-Wide Association Studies in Alzheimer's Disease. *Neurosci Bull.* 2016;32(2):183-190.
2. Karch CM, Goate AM. Alzheimer's disease risk genes and mechanisms of disease pathogenesis. *Biol Psychiatry.* 2015;77(1):43-51.
3. Guerreiro R, Hardy J. Genetics of Alzheimer's disease. *Neurotherapeutics.* 2014;11(4):732-737.
4. Bertram L, Tanzi RE. The genetics of Alzheimer's disease. *Prog Mol Biol Transl Sci.* 2012;107:79-100.
5. Rosenthal SL, Kamboh MI. Late-Onset Alzheimer's disease genes and the potentially implicated pathways. *Curr Genet Med Rep.* 2014;2:85-101.
6. Sims R, Van Der Lee SJ, Naj AC, et al. Rare coding variants in PLCG2, ABI3, and TREM2 implicate microglial-mediated innate immunity in Alzheimer's disease. *Nat Genet.* 2017;49(9):1373-1384.
7. Guerreiro R, Wojtas A, Bras J, et al. TREM2 variants in Alzheimer's disease. *N Engl J Med.* 2013;368(2):117-127.
8. Jonsson T, Stefansson H, Steinberg S, et al. Variant of TREM2 associated with the risk of Alzheimer's disease. *N Engl J Med.* 2013;368(2):107-116.
9. Koss H, Bunney TD., Behjati S, Katan M. Dysfunction of phospholipase Cγ in immune disorders and cancer. *Trends in Biochemical Sciences*, 2014;39(12):603–611. http://doi.org/10.1016/j.tibs.2014.09.004
10. Magno L, Lessard CB, Martins M, et al. Alzheimer's disease phospholipase C-gamma-2 (PLCG2) protective variant is a functional hypermorph. *Alzheimers Res Ther.* 2019;11(1):16.
11. Takalo M, Wittrahm R, Wefers B, et al. The Alzheimer's disease-associated protective Plcgamma2-P522R variant promotes immune functions. *Mol Neurodegener.* 2020;15(1):52.
12. Maguire E, Menzies GE, Phillips T, et al. PIP2 depletion and altered endocytosis caused by expression of Alzheimer's disease-protective variant PLCgamma2 R522. *EMBO J.* 2021;40(17):e105603.
13. Mcquade A, Coburn M, Tu CH, Hasselmann J, Davtyan H, Blurton-Jones M. Development and validation of a simplified method to generate human microglia from pluripotent stem cells. *Mol Neurodegener.* 2018;13(1):67.
14. Hasselmann J, Coburn MA, England W. Development of a chimeric model to study and manipulate human microglia in vivo. *Neuron.* 2019;103(6):1016-1033.e10. e10.

15. Devaiah BN, Singer DS. CIITA and its dual roles in MHC gene transcription. *Front Immunol*. 2013;4:476.

16. Martin BK, Chin K-C, Olsen JC, et al. Induction of MHC class I expression by the MHC class II transactivator CIITA. *Immunity*. 1997;6(5):591-600.

17. Handunnetthi L, Ramagopalan SV, Ebers GC, Knight JC. Regulation of major histocompatibility complex class II gene expression, genetic variation and disease. *Genes Immun*. 2010;11(2):99-112.

18. Olah M, Menon V, Habib N, et al. Single cell RNA sequencing of human microglia uncovers a subset associated with Alzheimer's disease. *Nat Commun*. 2020;11(1):6129.

19. Lu R-C, Yang Wu, Tan L, et al. Association of HLA-DRB1 polymorphism with Alzheimer's disease: a replication and meta-analysis. *Oncotarget*. 2017;8(54):93219-93226.

20. Lambert J-C, Ibrahim-Verbaas CA, Harold D, et al. Meta-analysis of 74,046 individuals identifies 11 new susceptibility loci for Alzheimer's disease. *Nat Genet*. 2013;45(12):1452-1458.

21. Mittal K, Eremenko E, Berner O, et al. CD4 T cells induce a subset of MHCII-Expressing microglia that attenuates Alzheimer's pathology. *iScience*. 2019;16:298-311.

22. Evans FL, Dittmer M, De La Fuente AG, Fitzgerald DC. Protective and regenerative roles of T cells in central nervous system disorders. *Front Immunol*. 2019;10:2171.

23. Gate D, Saligrama N, Leventhal O, et al. Clonally expanded CD8 T cells patrol the cerebrospinal fluid in Alzheimer's disease. *Nature*. 2020;577(7790):399-404.

24. Rogers J, Luber-Narod J, Styren SD, Civin WH. Expression of immune system-associated antigens by cells of the human central nervous system: relationship to the pathology of Alzheimer's disease. *Neurobiol Aging*. 1988;9(4):339-349.

25. Mutnal MB, Hu S, Little MR, Lokensgard JR. Memory T cells persisting in the brain following MCMV infection induce long-term microglial activation via interferon-gamma. *J Neurovirol*. 2011;17(5):424-437.

26. Britschgi M, Olin CE, Johns HT, et al. Neuroprotective natural antibodies to assemblies of amyloidogenic peptides decrease with normal aging and advancing Alzheimer's disease. *Proc Natl Acad Sci U S A*. 2009;106(29):12145-12150.

27. Wang S, Mustafa M, Yuede CM, et al. Anti-human TREM2 induces microglia proliferation and reduces pathology in an Alzheimer's disease model. *J Exp Med*. 2020;217(9).

28. Schlepckow K, Monroe KM, Kleinberger G, et al. Enhancing protective microglial activities with a dual function TREM2 antibody to the stalk region. *EMBO Mol Med*. 2020;12(4):e11227.

29. Yu P, Constien R, Dear N, et al. Autoimmunity and inflammation due to a gain-of-function mutation in phospholipase C gamma 2 that specifically increases external Ca2+ entry. *Immunity*. 2005;22(4):451-465.

30. Mcquade A, Kang YJ, Hasselmann J, et al. Gene expression and functional deficits underlie TREM2-knockout microglia responses in human models of Alzheimer's disease. *Nat Commun*. 2020;11(1):5370.

31. Oakley H, Cole SL, Logan S, et al. Intraneuronal beta-amyloid aggregates, neurodegeneration, and neuron loss in transgenic mice with five familial Alzheimer's disease mutations: potential factors in amyloid plaque formation. *J Neurosci*. 2006;26(40):10129-10140.

32. Butler A, Hoffman P, Smibert P, Papalexi E, Satija R. Integrating single-cell transcriptomic data across different conditions, technologies, and species. *Nat Biotechnol*. 2018;36(5):411-420.

33. Trapnell C, Cacchiarelli D, Grimsby J, et al. The dynamics and regulators of cell fate decisions are revealed by pseudotemporal ordering of single cells. *Nat Biotechnol*. 2014;32(4):381-386.

34. Bolger AM, Lohse M, Usadel B. Trimmomatic: a flexible trimmer for Illumina sequence data. *Bioinformatics*. 2014;30(15):2114-2120.

35. Bray NL, Pimentel H, Melsted P, Pachter L. Near-optimal probabilistic RNA-seq quantification. *Nat Biotechnol*. 2016;34(5):525-527.

36. Love MI, Huber W, Anders S. Moderated estimation of fold change and dispersion for RNA-seq data with DESeq2. *Genome Biol*. 2014;15(12):550.

37. Khan A, Fornes O, Stigliani A, et al. JASPAR 2018: update of the open-access database of transcription factor binding profiles and its web framework. *Nucleic Acids Res*. 2018;46(D1):D260-D266.

38. Mi H, Muruganujan A, Thomas PD. PANTHER in 2013: modeling the evolution of gene function, and other gene attributes, in the context of phylogenetic trees. *Nucleic Acids Res*. 2013;41(Database issue):D377-D386.

39. Merico D, Isserlin R, Stueker O, Emili A, Bader GD. Enrichment map: a network-based method for gene-set enrichment visualization and interpretation. *PLoS One*. 2010;5(11):e13984.

40. Shannon P, Markiel A, Ozier O, et al. Cytoscape: a software environment for integrated models of biomolecular interaction networks. *Genome Res*. 2003;13(11):2498-2504.

41. Gómez-Rubio V. (2017) ggplot2 - Elegant Graphics for Data Analysis (2nd Edition). *Journal of Statistical Software*, 77, (Book Review 2), http://doi.org/10.18637/jss.v077.b02

42. Keren-Shaul H, Spinrad A, Weiner A, et al. A Unique Microglia Type Associated with Restricting Development of Alzheimer's Disease. *Cell*. 2017;169(7):1276-1290.e17. e17.

43. Farbehi N, Patrick R, Dorison A, et al. Single-cell expression profiling reveals dynamic flux of cardiac stromal, vascular and immune cells in health and injury. *Elife*. 2019;8.

SUPPORTING INFORMATION

Additional supporting information may be found in the online version of the article at the publisher's website.